A Stable Adaptive Attitude Estimator on $SO(3)$ for True-North Seeking Gyrocompass Systems: Theory and Preliminary Simulation Evaluation

Andrew R. Spielvogel and Louis L. Whitcomb

***Abstract*— This paper reports a novel stable adaptive attitude estimator and preliminary simulation results of a true-North gyrocompass system employing the attitude adaptive identifier and a commercially available low-cost inertial measurement unit (IMU) comprising a 3-axis fiber optic gyroscope (FOG) with a 3-axis micro-electro-mechanical systems (MEMS) accelerometer. Optical North-seeking gyrocompass systems typically employ a microprocessor system to sample the low-level raw sensor values for angular-rate and linear-acceleration at a high sampling rate and estimate true-North heading, pitch, and roll. This paper reports the first adaptive attitude estimator on $SO(3)$ which utilizes 3-axis angular-rate sensor data and 3-axis linear acceleration sensor data to estimate the instrument's 3-degrees of freedom (DOF) attitude (roll, pitch, and heading) without using magnetometry of the Earth's magnetic field. A stability proof and preliminary numerical simulation results are reported. The simulation results for a rotating IMU configuration are promising, and further experimental evaluation and extension of the algorithm for the case of a translating IMU configuration typically found on moving robotic vehicles are needed.**

I. Introduction

Accurate true-North heading and attitude measurement is a critical component of high-accuracy navigation systems for a wide variety of robotic vehicles. The need for accurate true-North heading and attitude estimation is particularly acute in the case of vehicles operating in global positioning system (GPS)-denied environments (such as underwater) and in magnetically compromised environments (such as near ferromagnetic structures, buildings, or natural local magnetic anomalies). Smaller and lower-cost vehicles represent an additional challenge due to their limited sensor budget, small physical size, and limited energy storage capacity.

Over the past decade, for example, the development of a new generation of small low-cost underwater vehicles (UVs) has begun to enable oceanographic, environmental assessment, and national security missions that were considered impractical or infeasible before (e.g. [2], [3], [11], [14], [17]). This new generation of UVs often employ low-cost navigation systems that presently limit them to missions requiring only low-precision navigation of $\mathcal{O}$(10-100)m accuracy. High-end navigation approaches, of $\mathcal{O}$(0.1-10)m accuracy, traditionally require a Doppler sonar, costing \$20k-\$50k, and a North-seeking gyrocompass or inertial navigation system (INS), costing \$50k-\$250k. These high-end navigation approaches are largely incompatible with low-cost autonomous underwater vehicles (AUVs) with target total vehicle cost of \$50k-\$250k.

Small low-cost UVs typically employ micro-electro-mechanical systems (MEMS) inertial measurement units (IMUs) comprised of 3-axis MEMS magnetometers and 3-axis MEMS accelerometers to estimate local magnetic heading, pitch, and roll to within several degrees of accuracy. Studies have shown that the accuracy of these magnetic heading sensors can be a principal error source in overall navigation solutions [6].

These low-accuracy attitude sensors limit the navigation accuracy of small underwater vehicles. The high cost, large size, and high power-consumption of optical true-North seeking gyrocompasses is a principal barrier to the widespread use of high accuracy navigation for smaller and lower-cost UVs.

Recently, a new class of low-cost fiber optic gyroscope (FOG) IMUs have become available — for example the commercial-off-the-shelf (COTS) KVH 1775 IMU (KVH Industries, Inc., Middletown, RI, USA) — that provide sensor accuracies sufficient for estimation of true-North heading, pitch and roll. Recent work by Costanzi et al. has developed an attitude estimation algorithm under unknown magnetic disturbances utilizing a low-cost FOG [4]. [4] differs from this paper as it estimates magnetic north while this paper presents an estimator for true-North heading.

A previously published study by the authors reports the results of a preliminary experimental evaluation of a *static* (non-rotating) configuration of a low-cost IMU, suggesting their possible practical utility as the primary sensor in a North-seeking gyrocompass system [13].

The present paper reports a new stable algorithm for estimating attitude of a *dynamic* (rotating) *IMU* along with preliminary simulation results of the identifier employing a low-cost FOG IMU as the primary sensor.

This paper is organized as follows: Section II gives an overview of preliminaries. Section III reports the novel attitude adaptive identifier. Section IV presents numerical simulations. Section V summarizes and concludes.

II. Preliminaries

A. Coordinate Frames

We define the following coordinate frames:

Instrument Frame: A frame (i) fixed in the IMU instrument.

Zero Frame: The zero frame (z) is the instrument frame at t_0.

We gratefully acknowledge the support of the National Science Foundation under NSF award OCE-1435818. The authors are with the Department of Mechanical Engineering, Johns Hopkins University, Baltimore, MD 21218, USA. Email: {aspielv1,llw}@jhu.edu

North-East-Down (NED) Frame: The North-East-Down (NED) frame (N) has its x-axis pointing North, its y-axis pointing East, its z-axis pointing down, and its origin co-located with that of the instrument frame.

B. Notation and Definitions

For each vector, a leading superscript indicates the frame of reference and a following subscript indicates the signal source, thus ${}^{N}w_m$ is the measured instrument angular velocity in the NED frame and ${}^{i}a_m$ is the measured instrument linear acceleration in the instrument sensor frame.

Definition: The set of 3×3 rotation matrices forms a group, known as the special orthogonal group, SO(3), defined as

$$SO(3) = \{R : R \in \mathbb{R}^{3\times3}, R^T R = I_{3\times3}, \det(R) = 1\}. \quad (1)$$

For each rotation matrix a leading superscript and subscript indicates the frames of reference. For example, ${}^{N}_{i}R$ is the rotation from the instrument frame to the NED frame.

The elements of a rotation matrix $R \in SO(3)$ are defined with following subscripts,

$$R = \begin{bmatrix} R_{11} & R_{12} & R_{13} \\ R_{21} & R_{22} & R_{23} \\ R_{31} & R_{32} & R_{33} \end{bmatrix}. \quad (2)$$

Definition: The set of 3×3 skew-symmetric matrices is defined as

$$so(3) = \{S : S \in \mathbb{R}^{3\times3}, S^T = -S\}. \quad (3)$$

Definition: J is defined as a function that maps a 3×1 vector to the corresponding 3×3 skew-symmetric matrix, $J : \mathbb{R}^3 \to so(3)$. For $k \in \mathbb{R}^3$

$$J(k) = \begin{bmatrix} 0 & -k_3 & k_2 \\ k_3 & 0 & -k_1 \\ -k_2 & k_1 & 0 \end{bmatrix} \quad (4)$$

We define its inverse $J^{-1} : so(3) \to \mathbb{R}^3$, such that $\forall x \in \mathbb{R}^3$, $J^{-1}(J(x)) = x$.

C. Sensor Model

The sensor data is modeled as

$$ {}^{i}w_m(t) = {}^{i}w_E(t) + {}^{i}w_v(t) + {}^{i}w_b + {}^{i}\eta_w(t) \quad (5)$$
$$ {}^{i}a_m(t) = {}^{i}a_g(t) + {}^{i}a_v(t) + {}^{i}a_b + {}^{i}\eta_a(t) \quad (6)$$
$$ {}^{i}w_e(t) = {}^{i}w_E(t) + {}^{i}w_v(t) + {}^{i}w_b \quad (7)$$
$$ {}^{i}a_e(t) = {}^{i}a_g(t) + {}^{i}a_v(t) + {}^{i}a_b \quad (8)$$

where ${}^{i}w_m(t)$ is the IMU measured angular-rate, ${}^{i}w_e(t)$ is the expected angular-rate, ${}^{i}w_E(t)$ is the true angular velocity due to the rotation of the Earth, ${}^{i}w_v(t)$ is the true angular velocity due to the rotation of the instrument with respect to the NED frame, ${}^{i}w_b$ is the angular velocity sensor bias offset, ${}^{i}\eta_w(t)$ is the zero-mean Gaussian angular velocity sensor noise, ${}^{i}a_m(t)$ is the IMU measured linear acceleration, ${}^{i}a_e(t)$ is the expected linear acceleration, ${}^{i}a_g(t)$ is the true linear acceleration due to gravity and the Earth's rotation, ${}^{i}a_v(t)$ is the instrument's true linear acceleration with respect to Earth, ${}^{i}a_b$ is the linear accelerometer sensor bias, and ${}^{i}\eta_a(t)$ is the zero-mean Gaussian linear accelerometer sensor noise. Angular velocity sensor and linear accelerometer sensor noises are computed from the IMU manufacturer's specifications [9], as per [16], and confirmed experimentally ($\sigma_w = 6.32 \times 10^{-3}$ rad/s, $\sigma_a = 0.0037$ g).

Accurate on-line sensor bias compensation is important to the accuracy of the proposed algorithm, but is beyond the scope of the present conference paper. Troni and Whitcomb present an adaptive estimator for determining 3-axes magnetometer and 3-axes linear accelerometer biases in [15]. However, stable simultaneous on-line sensor bias compensation for accelerometers and angular rate gyros remains a non-trivial problem and is the subject of a separate paper presently in preparation. Thus, for the numerical simulation results reported herein, we assume that the bias offset has been accurately estimated and compensated. In addition, we assume that the instrument is only rotating with respect to the NED frame (${}^{i}a_v(t) = 0$). With these assumptions, the sensor data model simplifies to

$$ {}^{i}w_m(t) = {}^{i}w_E(t) + {}^{i}w_v(t) + {}^{i}\eta_w(t) \quad (9)$$
$$ {}^{i}a_m(t) = {}^{i}a_g(t) + {}^{i}\eta_a(t) \quad (10)$$
$$ {}^{i}w_e(t) = {}^{i}w_E(t) + {}^{i}w_v(t) \quad (11)$$
$$ {}^{i}a_e(t) = {}^{i}a_g(t). \quad (12)$$

D. Mathematical Background

Proposition: For $Q(t) \in so(3)$, the rotation matrix $R(t)$ can be computed by Rodrigues' Equation [10]

$$R(Q(t)) = I_{3\times3} + \gamma(t)Q(t) + \kappa(t)Q(t)^2 \quad (13)$$

where

$$q(t) = J^{-1}(Q(t)) \quad (14)$$
$$\gamma(t) = \frac{\sin(\|q(t)\|)}{\|q(t)\|} \quad (15)$$
$$\kappa(t) = \frac{1 - \cos(\|q(t)\|)}{\|q(t)\|^2}. \quad (16)$$

Proposition: $\dot{q}(t)$ is related to $\dot{R}(t)$ by the mapping

$$R^T(t)\dot{R}(t) = J(A(q(t))\dot{q}(t)) \quad (17)$$

where $A(q(t))$ is the right Jacobian of $R(q(t)) = e^{J(q(t))}$ with respect to the angular position vector $q(t) \in \mathbb{R}^3$. $A(q(t))$ and its inverse,

$$A^{-1}(q(t)) = I_{3\times3} + \alpha(t)J(q(t)) + \beta(t)J(q(t))^2 \quad (18)$$

where

$$\alpha(t) = -\frac{1}{2}, \quad (19)$$
$$\beta(t) = \frac{1}{\|q(t)\|} - \frac{1 + \cos(\|q(t)\|)}{2\|q(t)\|\sin(\|q(t)\|)}, \quad (20)$$

are reported by Park in [12].

If $A(q(t))$ is invertible, (17) can be rearranged as

$$\dot{q}(t) = A^{-1}(q(t))\, J^{-1}\left(R^T(t)\dot{R}(t)\right) \quad (21)$$

and thus

$$\dot{Q}(t) = J\left(A^{-1}\left(q(t)\right) J^{-1}\left(R^T(t)\dot{R}(t)\right)\right). \quad (22)$$

Proposition: $\forall y(t) \in \mathbb{R}^3$ and $Q(t) = J(q(t))$ the following equality holds [8], [7]:

$$-\frac{1}{2}Tr\left(J\left(A^{-1}(q(t))y(t)\right)Q(t)\right) = q^T(t)y(t). \quad (23)$$

Proposition: The time derivative of gravity vector in the instrument frame can be computed by

$${}^i\dot{a}_g(t) = -J({}^iw_v(t)){}^ia_g(t). \quad (24)$$

Proof: Start with the relation between ${}^Na_g$ and ${}^ia_g(t)$

$${}^Na_g = {}^N_iR(t){}^ia_g(t). \quad (25)$$

Taking the time derivative of (25) and rearranging terms results in

$$\begin{aligned} 0 &= {}^N_iR(t)J({}^iw_v(t)){}^ia_g(t) + {}^N_iR(t){}^i\dot{a}_g(t) \\ {}^i\dot{a}_g(t) &= -J({}^iw_v(t)){}^ia_g(t). \end{aligned} \quad (26)$$

Proposition: The east vector can be computed by

$${}^ie_e(t) = J({}^iw_e(t)){}^ia_g(t) + {}^i\dot{a}_g(t). \quad (27)$$

Proof: Start with the fact that

$$\begin{aligned} {}^ie_e(t) &= {}^iw_E(t) \times {}^ia_g(t) \\ &= J({}^iw_E(t)){}^ia_g(t). \end{aligned} \quad (28)$$

substituting (11) into (28) results in

$${}^ie_e(t) = J({}^iw_e(t)){}^ia_g(t) - J({}^iw_v(t)){}^ia_g(t). \quad (29)$$

Then substituting (24) into (29) results in

$${}^ie_e(t) = J({}^iw_e(t)){}^ia_g(t) + {}^i\dot{a}_g(t). \quad (30)$$

III. A Novel Attitude Adaptive Identifier

This section reports a novel attitude adaptive identifier (roll, pitch, heading) based upon the adaptive identifier on $SO(3)$ reported by Kinsey and Whitcomb in [8], [7]. An additional error term has been developed to enable heading estimation.

A. Identifier Derivation

1) Plant: Define ${}^Na_e(t)$ and ${}^Ne_e(t)$ to be

$$\begin{aligned} {}^Na_e(t) &= {}^N_iR(t){}^ia_e(t) \\ &= {}^N_zR\ {}^z_iR(t){}^ia_e(t) \\ {}^Ne_e(t) &= {}^N_iR(t){}^ie_e(t) \\ &= {}^N_zR\ {}^z_iR(t){}^ie_e(t). \end{aligned} \quad (31)\ (32)$$

We consider the plant

$${}^Na_e(t) + {}^Ne_e(t) = {}^N_iR(t)\left({}^ia_e(t) + {}^ie_e(t)\right) \quad (33)$$

By separating ${}^N_iR(t)$ into the two rotations ${}^N_zR$ and ${}^z_iR(t)$, the plant can be rewritten as

$${}^Na_e(t) + {}^Ne_e(t) = {}^N_zR\left({}^za_e(t) + {}^ze_e(t)\right) \quad (34)$$

where ${}^Na_e(t)$ and ${}^Ne_e(t)$ are deterministic, ${}^ia_e(t)$ is the gravity vector, ${}^za_e(t) = {}^z_iR(t){}^ia_e(t)$, ${}^ze_e(t) = {}^z_iR(t){}^ie_e(t)$, ${}^z_iR(t)$ is computed by

$${}^z_iR(t) = \int_{t_0}^{t} {}^z_iR(\tau)J\left({}^iw_i(\tau)\right)\,d\tau,\ {}^z_iR(t_0) = I_{3\times3}, \quad (35)$$

and ${}^ie_e(t)$ is computed by (27).

2) Identification Plant: Define ${}^N_z\hat{R}(t) \in SO(3)$ to be the estimate of ${}^N_zR$, and ${}^N\hat{a}_e(t)$ and ${}^N\hat{e}_e(t)$ to be

$${}^N\hat{a}_e(t) = {}^N_z\hat{R}{}^za_e(t) \quad (36)$$

$${}^N\hat{e}_e(t) = {}^N_z\hat{R}{}^ze_e(t). \quad (37)$$

The estimated plant output then is

$${}^N\hat{a}_e(t) + {}^N\hat{e}_e(t) = {}^N_z\hat{R}(t)\left({}^za_e(t) + {}^ze_e(t)\right). \quad (38)$$

3) Parameter Error: The parameter error is defined as

$$\tilde{R}(t) = {}^N_zR^T{}^N_z\hat{R}(t). \quad (39)$$

Since ${}^N_zR$ is constant,

$$\dot{\tilde{R}}(t) = {}^N_zR^T{}^N_z\dot{\hat{R}}(t). \quad (40)$$

4) Output Error: The local level and heading output error terms are defined, respectively, as

$$\tilde{a}(t) = k_a{}^N_z\hat{R}^T(t)\left({}^N\hat{a}_e(t) \times {}^Na\right) \quad (41)$$

$$\tilde{e}(t) = k_w{}^N_z\hat{R}^T(t){}^N\bar{a}{}^N\bar{a}^T\left({}^N\hat{e}_e(t) \times {}^Ne\right) \quad (42)$$

where

$${}^Na = \left(I_{3\times3} + \frac{1}{g_0}J({}^Nw_E)^2\right)\begin{bmatrix}0 & 0 & -1\end{bmatrix}^T, \quad (43)$$

$${}^N\bar{a} = \frac{{}^Na}{\|{}^Na\|}, \quad (44)$$

$${}^Ne = {}^Nw_E \times {}^Na, \quad (45)$$

g_0 is the magnitude of the gravity vector, and $k_a > 0$ and $k_w > 0$ are constants. Note that ${}^N\hat{a}_e(t) \times {}^Na = 0$ and ${}^N\hat{e}_e(t) \times {}^Ne = 0$ when the estimated and actual plant outputs are aligned. The output error can be represented as skew-symmetric matrices where the terms are defined as

$$\tilde{A}(t) = J(\tilde{a}(t)), \quad (46)$$

$$\tilde{E}(t) = J(\tilde{e}(t)). \quad (47)$$

5) Update Law: We choose the update law

$${}^N_z\dot{\hat{R}}(t) = {}^N_z\hat{R}(t)\left(\tilde{A}(t) + \tilde{E}(t)\right). \quad (48)$$

6) System: The resulting system from substituting (48) into (40) is

$$\begin{aligned} \dot{\tilde{R}}(t) &= {}^N_zR^T\ {}^N_z\dot{\hat{R}}(t) \\ &= {}^N_zR^T\ {}^N_z\hat{R}(t)\left(\tilde{A}(t) + \tilde{E}(t)\right) \\ &= \tilde{R}(t)\left(\tilde{A}(t) + \tilde{E}(t)\right). \end{aligned} \quad (49)$$

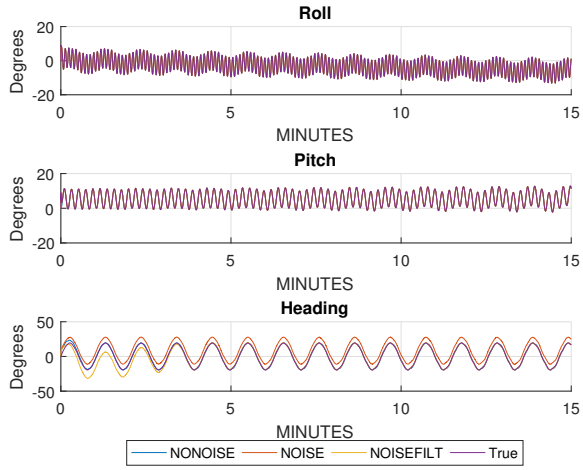

Fig. 1. Simulation attitude estimates.

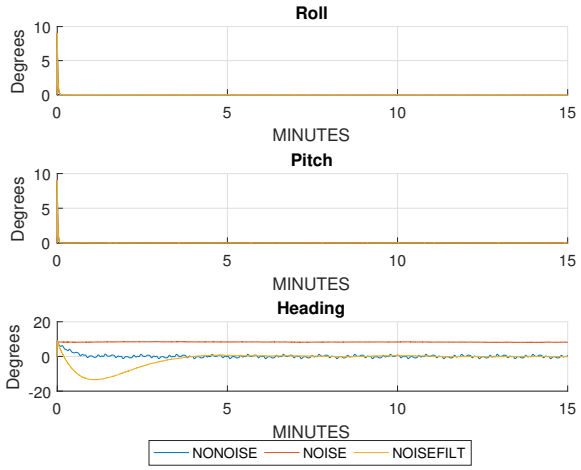

Fig. 2. Simulation attitude estimates' error.

7) Stability: The Lyapunov candidate function is [1]

$$\begin{aligned} V(\tilde{R}(t)) &= \|\tilde{R}(t)\|^2_{SO(3)} \\ &= -\frac{1}{2}Tr(\tilde{Q}(t)\tilde{Q}(t)) \\ &= \|\tilde{q}(t)\|^2 \end{aligned} \tag{50}$$

where $\tilde{Q}(t) = \ln(\tilde{R}(t))$ and $\tilde{q}(t) = J^{-1}(\tilde{Q}(t))$. $V : SO(3) \to \mathbb{R}^1$ is a smooth function in the neighborhood of the identity rotation $I_{3\times3}$, $V(I_{3\times3}) = 0$, and $V(R) > 0$ if $R \neq I_{3\times3}$ in the neighborhood of $I_{3\times3}$ [1].

Taking the time derivative and substituting in (22) and (49) yields [1], [5]

$$\begin{aligned} \dot{V}(\tilde{R}(t)) &= -Tr(\dot{\tilde{Q}}(t)\tilde{Q}(t)) \\ &= -Tr\left(J(A^{-1}(\tilde{q}(t))(\tilde{u}(t)))\tilde{Q}(t)\right). \end{aligned} \tag{51}$$

where

$$\tilde{u}(t) = \tilde{a}(t) + \tilde{e}(t). \tag{52}$$

Using (23) and the fact that orthogonal matrices distribute over the cross product results in

$$\begin{aligned} \dot{V}(\tilde{R}(t)) &= 2\tilde{q}^T(t)\left(\tilde{a}(t) + \tilde{e}(t)\right) \\ &= 2k_a\tilde{q}^T(t){}^N_z\hat{R}^T(t)\left({}^N\hat{a}_e(t) \times {}^Na\right) \\ &\quad +2k_w\tilde{q}^T(t){}^N_z\hat{R}^T(t){}^N\bar{a}{}^N\bar{a}^T\left({}^N\hat{e}_e(t) \times {}^Ne\right) \\ &= 2k_a\tilde{q}^T(t)J\left({}^za_e(t)\right)\tilde{R}^T(t){}^za_e(t) \\ &\quad +2k_w\tilde{q}^T(t)\tilde{R}^T(t){}^z\bar{a}(t){}^z\bar{a}^T(t)\tilde{R}(t) \\ &\quad \left(J({}^ze_e(t))\tilde{R}^T(t){}^ze_e(t)\right) \\ &= 2k_a\tilde{q}^T(t)J\left({}^za_e(t)\right)\tilde{R}^T(t){}^za_e(t) \\ &\quad +2k_w\tilde{q}^T(t)PJ({}^ze_e(t))\tilde{R}^T(t){}^ze_e(t) \end{aligned} \tag{53}$$

where

$$P = \tilde{R}^T(t){}^z\bar{a}(t){}^z\bar{a}^T(t)\tilde{R}(t) \tag{54}$$

is a projection matrix.

Substituting (13) into (53) yields

$$\begin{aligned} \dot{V}(\tilde{R}(t)) &= 2k_a\tilde{q}^T(t)J\left({}^za_e(t)\right){}^za_e(t) \\ &\quad -2\tilde{\gamma}(t)k_a\tilde{q}^T(t)J\left({}^za_e(t)\right)J(\tilde{q}(t)){}^za_e(t) \\ &\quad +2\tilde{\kappa}(t)k_a\tilde{q}^T(t)J\left({}^za_e(t)\right)J^2(\tilde{q}(t)){}^za_e(t) \\ &\quad +2k_w\tilde{q}^T(t)PJ({}^ze_e(t)) \\ &\quad \left(I - \tilde{\gamma}(t)J(\tilde{q}(t)) + \tilde{\kappa}J(\tilde{q}(t))\right){}^ze_e(t) \\ &= -2k_a\tilde{\gamma}(t)\tilde{q}^T(t)J\left({}^za_e(t)\right)J(\tilde{q}(t)){}^za_e(t) \\ &\quad +2k_w\tilde{q}^T(t)PJ({}^z\bar{e}_e(t)) \\ &\quad \left(-\tilde{\gamma}(t)J(\tilde{q}(t)) + \tilde{\kappa}J^2(\tilde{q}(t))\right){}^z\bar{e}_e(t) \\ &= -2k_a\tilde{\gamma}(t)\tilde{q}^T(t)J\left({}^za_e(t)\right)J(\tilde{q}(t)){}^za_e(t) \\ &\quad +2k_w\tilde{\kappa}(t)\tilde{q}^T(t)PJ({}^ze_e(t))J^2(\tilde{q}(t)){}^ze_e(t) \\ &\quad +2k_w\tilde{\gamma}(t)\tilde{q}^T(t)PJ({}^ze_e(t))J({}^ze_e(t))\tilde{q}(t) \end{aligned} \tag{55}$$

Using the fact that $P^2 = P$ for projection matrices and orthogonal matrices distribute over the cross product, (55) becomes

$$\begin{aligned} \dot{V}(\tilde{R}(t)) &= -2k_a\tilde{\gamma}(t)\tilde{q}^T(t)J^T\left({}^za_e(t)\right)J({}^za_e(t))\tilde{q}(t) \\ &\quad -2k_w\tilde{\gamma}(t)\tilde{q}^T(t)P^TJ^T(P^ze_e(t))J(P^ze_e(t))P\tilde{q}(t) \\ &\quad +2k_w\tilde{\kappa}(t)\tilde{q}^T(t)P^TJ^T(P^ze_e(t)) \\ &\quad J(P\tilde{q}(t))J(P^ze_e(t))P\tilde{q}(t) \\ &= -2k_a\tilde{\gamma}(t)\|J\left({}^za_e(t)\right)\tilde{q}(t)\|^2 \\ &\quad -2k_w\tilde{\gamma}(t)\|J(P^ze_e(t))P\tilde{q}(t)\|^2. \end{aligned} \tag{56}$$

Hence, the time derivative of the Lyapunov function is negative semidefinite and the adaptive identifier is locally stable. Although additional arguments beyond the scope of this paper are required to show convergence of the attitude estimate, the numerical simulations show the attitude estimate to converge to the true attitude.

8) Attitude Calculation: Calculate the ${}^N_i\hat{R}(t)$ rotation:

$${}^N_i\hat{R}(t) = {}^N_z\hat{R}(t){}^z_iR(t). \tag{57}$$

Roll ($\phi(t)$), pitch ($\theta(t)$), and heading ($\gamma(t)$) estimations can be found by the usual formula

$$\begin{aligned}\gamma(t) &= \text{atan2}\left({}^N_i\hat{R}_{21}(t), {}^N_i\hat{R}_{11}(t)\right)\\ \theta(t) &= \text{atan2}(-{}^N_i\hat{R}_{31}(t),\\ &\quad {}^N_i\hat{R}_{11}(t)\cos(\gamma(t)) - {}^N_i\hat{R}_{21}(t)\sin(\gamma(t)))\\ \phi(t) &= \text{atan2}({}^N_i\hat{R}_{13}(t)\sin(\gamma(t)) - {}^N_i\hat{R}_{23}(t)\cos(\gamma(t)),\\ &\quad -{}^N_i\hat{R}_{12}(t)\sin(\gamma(t)) + {}^N_i\hat{R}_{22}(t)\cos(\gamma(t))).\end{aligned} \tag{58}$$

B. Adaptive Identifier for Local Level

If the $\tilde{E}(t)$ term is removed from the update law in the attitude adaptive identifier derived above, we get an adaptive identifier for local level (roll and pitch). Its derivation follows from the more general attitude adaptive identifier and results in the following system.

1) Plant:

$${}^N a_e(t) = {}^N_z R^z a_e(t) \tag{59}$$

2) Identification Plant:

$${}^N \hat{a}_e(t) = {}^N_z \hat{R}(t)^z a_e(t) \tag{60}$$

3) Output Error:

$$\tilde{a}(t) = k_a {}^N\hat{R}^T(t)\left({}^N\hat{a}_e(t) \times {}^N a\right) \tag{61}$$

4) System:

$$\dot{\tilde{R}}(t) = \tilde{R}(t)\tilde{A}(t) \tag{62}$$

5) Stability:

$$V(\tilde{R}(t)) = \|\tilde{R}(t)\|^2_{SO(3)} \tag{63}$$

$$\dot{V}(\tilde{R}(t)) = -2k_a\tilde{\gamma}(t)\|J\left({}^z a_e(t)\right)\tilde{q}(t)\|^2 \tag{64}$$

Additional arguments beyond the scope of this paper are required to show convergence of the estimate.

IV. Numerical Simulations

The performance of the attitude adaptive identifier was evaluated with numerical simulations. Section IV-A presents the simulation setup and Section IV-B reports the simulation results.

A. Simulation Setup

Three numerical simulations were implemented using two datasets. Both datasets were sampled at 5 kHz for 15 minutes and experienced the same instrument rotations. However, the first dataset, DATA1, was without sensor noise while the second dataset, DATA2, included sensor noise representative of the KVH 1775 IMU (used ${}^i a_m(t)$ and ${}^i w_m(t)$ instead of ${}^i a_e(t)$ and ${}^i w_e(t)$).

All three simulations use gains of $k_a = 1$ and $k_w = 0.05$. The NONOISE simulation implements the attitude adaptive identifier on the DATA1 dataset while NOISE implements the identifier on the DATA2 dataset. The third simulation, NOISEFILT, implements the identifier on the DATA2 dataset with a lowpass first order Butterworth filter ($f_{cutoff} = 0.005$ Hz) on the ${}^N\hat{e}_e(t)$ signal.

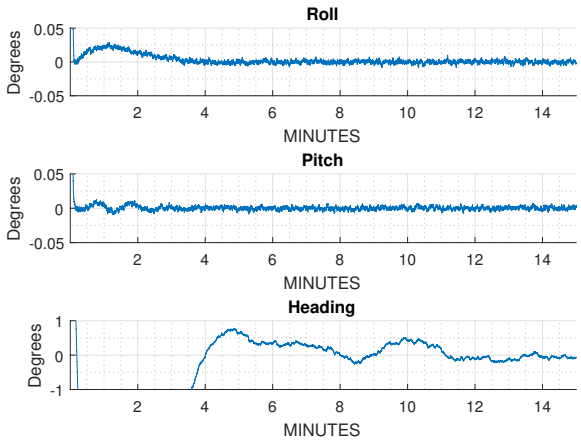

Fig. 3. NOISEFILT attitude estimate error.

B. Simulation Results

The attitude estimations for the three simulations are shown in Figure 1 and their corresponding errors in Figure 2. The simulation results show that the NONOISE case converges. However, the numerical differentiation of the acceleration signal introduces noise to the system which can be seen in Figure 2. In the NOISE simulation, the heading estimate does not converge during the 15 minute simulation. The authors believe this is because the signal to noise ratio is low due to the differentiation of the noisy acceleration signal. Hence for the NOISEFILT simulation, the ${}^N\hat{e}_e(t)$ signal was put through the lowpass Butterworth filter. As shown in Figure 2, the NOISEFILT attitude estimation converges to the true value. Figure 3 shows that the heading estimation is within 0.3° and the roll and pitch are within 0.01° of the true values after 15 minutes of running the adaptive identifier.

V. Conclusion

This paper reports a novel stable adaptive attitude estimator and preliminary simulation evaluations based on the noise characteristics of the commercially available low-cost KVH 1775 IMU's data-sheet. The simulation results of a rotating system employing a low-cost FOG IMU indicates that the algorithm can successfully find true-North if the sensor bias offsets have accurately been compensated. Overall, these data suggest the convergence of the adaptive identifier's attitude estimate to the true attitude for the case of a rotating IMU configuration. In future studies, we hope to experimentally evaluate the adaptive identifier, develop real-time 6-degrees of freedom (DOF) IMU bias estimation, and address the general-use-case of the simultaneously rotating and translating instrument configuration.

References

[1] F. Bullo and R. Murray. Proportional derivative control on the Euclidean group. Technical report, California Institute of Technology, Anaheim, CA USA, 1995.

[2] D. Clegg and M. Peterson. User operational evaluation system of unmanned underwater vehicles for very shallow water mine countermeasures. In *Proceedings of IEEE/MTS OCEANS 2003*, volume 3, pages 1417–1423 Vol.3, Sept 2003.

[3] T. Clem, D. Sternlicht, J. Fernandez, J. Prater, R. Holtzapple, R. Gibson, J. Klose, and T. Marston. Demonstration of advanced sensors for underwater unexploded ordnance (UXO) detection. In *Proceedings of IEEE/MTS OCEANS 2012*, pages 1–4, Oct 2012.

[4] R. Costanzi, F. Fanelli, N. Monni, A. Ridolfi, and B. Allotta. An attitude estimation algorithm for mobile robots under unknown magnetic disturbances. *IEEE/ASME Transactions on Mechatronics*, 21(4):1900–1911, Aug 2016.

[5] J. C. Kinsey. *Advances in Precision Navigation of Oceanographic Submersibles*. PhD thesis, The Johns Hopkins University, Baltimore, MD USA, June 2006.

[6] J. C. Kinsey and L. L. Whitcomb. Preliminary field experience with the DVLNAV integrated navigation system for oceanographic submersibles. *Control Engineering Practice*, 12(12):1541–1548, December 2004. Invited Paper.

[7] J. C. Kinsey and L. L. Whitcomb. Adaptive identification on the group of rigid body rotations. In *Proceedings of the 2005 IEEE International Conference on Robotics and Automation*, pages 3256–3261, April 2005.

[8] J. C. Kinsey and L. L. Whitcomb. Adaptive identification on the group of rigid-body rotations and its application to underwater vehicle navigation. *IEEE Transactions on Robotics*, 23(1):124–136, Feb 2007.

[9] KVH Industries, Inc., Middletown, RI, USA. The KVH web site http://www.kvh.com and KVH 1775 IMU specifications sheet http://www.kvh.com/viewattachment.aspx?guidid=DFB3BCDF-CFA1-422D-837A-92F4F68D9BE5, 2015.

[10] R. M. Murray, Z. Li, and S. S. Sastry. *A Mathematical Introduction to Robotic Manipulation*. CRC Press, 1994.

[11] G. Packard, A. Kukulya, T. Austin, M. Dennett, R. Littlefield, G. Packard, M. Purcell, R. Stokey, and G. Skomal. Continuous autonomous tracking and imaging of white sharks and basking sharks using a REMUS-100 AUV. In *Oceans - San Diego, 2013*, pages 1–5, Sept 2013.

[12] F. Park. *The Optimal Kinematic Design of Mechanisms*. PhD thesis, Harvard University, Cambridge, MA USA, May 1991.

[13] A. R. Spielvogel and L. L. Whitcomb. Preliminary results with a low-cost fiber-optic gyrocompass system. In *OCEANS 2015 - MTS/IEEE Washington*, pages 1–5, Oct 2015.

[14] E. Steele, T. Boyd, M. Inall, E. Dumont, and C. Griffiths. Cooling of the West Spitsbergen Current: AUV-based turbulence measurements west of Svalbard. In *Autonomous Underwater Vehicles (AUV), 2012 IEEE/OES*, pages 1–7, Sept 2012.

[15] G. Troni and L. L. Whitcomb. Adaptive estimation of measurement bias in three-dimensional field sensors with angular rate sensors: Theory and comparative experimental evaluation. In *Robotics: Science and Systems*, 2013.

[16] Woodman, Oliver J. An introduction to inertial navigation. Technical report, University of Cambridge, Cambridge, UK, 2007.

[17] M. Zhou, R. Bachmayer, and B. de Young. Working towards seafloor and underwater iceberg mapping with a Slocum glider. In *Autonomous Underwater Vehicles (AUV), 2014 IEEE/OES*, pages 1–5, Oct 2014.